LIQUEFACTION, LATERAL SPREADING AND FLOW SLIDES

Mahmood Seid-Karbasi, Civil Engineering Department, University of British Columbia, Vancouver, Canada
Peter M. Byrne, Civil Engineering Department, University of British Columbia, Vancouver, Canada

ABSTRACT
Experience from past earthquakes indicates that large lateral spreads and flow slides in alluvial sand deposits have taken place in coastal and river areas in many parts of the world. The ground slope in these slides was often not very steep, gentler than a few percent. Recent research indicates that the presence of low permeability silt or clay sub layers is responsible for this behavior. Such layers form a barrier to flow of water associated with earthquake generated pore pressures causing an accumulation of pore water at the base of the layers, resulting in greatly reduced strength and possible slope instability. This paper uses an effective stress coupled stress flow dynamic analyses procedure to demonstrate the effects of a low permeability barrier layer on ground deformations from an earthquake event. It is shown that a slight inclination of the ground can result in flow failure and large deformations when a barrier layer is present. Without such a layer, the slope is quite stable. The slope with barrier layer can be stabilized by drains.

RE`SUME`
L'expérience des tremblements de terre passés indique que d'importants étalements latéraux et des coulées dans des dépôts alluvionnaires de sable ont eu lieu dans les zones côtières et fluviales de plusieurs régions du monde. La pente du terrain dans ces glissements était souvent peu prononcée. Les travaux récents indiquent que la présence de sous-couches de silt ou d'argile ayant une faible perméabilité est la cause de ce comportement. De telles couches forment une barrière qui empêche l'écoulement de l'eau lié aux pressions interstitielles produites par le tremblement de terre ; ceci cause une accumulation de l'eau interstitielle à la base des couches et entraîne une réduction importante de la résistance et l'instabilité possible de la pente. Dans cet article, on emploie une méthode d'analyses dynamiques en contrainte effective couplant les contraintes et les écoulements. Ce procédé est utilisé pour démontrer les effets d'une couche-barrière de faible perméabilité sur les déformations du sol lors d'un tremblement de terre. On montre qu'une légère inclinaison du terrain peut avoir comme conséquence une coulée et de grandes déformations quand une couche-barrière est présente. Sans une telle couche, la pente est relativement stable. Une pente comportant une couche-barrière peut être stabilisée à l'aide de drains.

1. INTRODUCTION

Experience from past earthquakes indicates that lateral spreads and flow slides have taken place in liquefied ground in coastal and river areas in many regions of the world including Alaska, Niigata, and Turkey. Movements may exceed several meters even in gentle slopes of less than a few percent (Kokusho 2003). Submarine slides have been seismically triggered in many regions as reported by Scott and Zukerman (1972) and Hamada (1992). More interestingly, lateral spreads or flow slides have occurred not only during, but also after earthquake shaking. These large movements are mainly driven by gravity, although initially triggered to liquefy by seismic stresses.

In the Hakusan District in Niigata city, an area 250 m x 150 m bordering the Shinano River moved toward the river during the 1964 Niigata earthquake in Japan (Kawakami and Asada 1966). Girders of the Showa Ohashi Bridge fell down due to flow failure of the liquefied riverbed that moved the supporting pile foundations. Eyewitnesses reported that the girders began to fall a few minutes after the earthquake motion had ceased (Hamada 1992). At the Lower San Fernando dam, a hydraulic fill in California, flow failure due to liquefaction in the upstream slope occurred about a half minute after the strong shaking in the 1971 earthquake (Seed 1987). Mochikoshi tailings dams in Japan failed as a result of the 1978 Izu-Ohshim-Kinkai earthquake due to liquefaction induced flow slides, causing release of the tailings (Ishihara 1984). One dam failed during the shaking, while a second failed 24 hours later.

Flow failures in liquefied soil deposits have also occurred in submarine slides triggered by earthquakes. The slopes in these slides were more gentle, normally less than 5^{o} and sometimes less than 1^{o} (Hampton and Lee, 1996). During the 1964 Alaska earthquake, Valdez and Seward port cities suffered great loss of life and property from large-scale submarine slides (Coulter and Migliaccio 1966 and Lemke 1967). In the 1999 Kocaeli earthquake, Turkey, widespread large lateral spreads are reported by Kokusho (2003). Coastal areas along Izmit Bay suffered submarine slides triggered by the earthquake. The ground inclination in these cases was low. During 1980 Mammoth lakes earthquake in California, a 2 km x 20 km area of sea floor, consisting of sand and mud on a slope of 0.25^{o}, suffered a flow slide. There was evidence of liquefaction in the form of sand boils on the sea floor. (Field et al.1982).

Although lateral flow failures have been reported in past earthquakes causing damage to structures, the mechanism leading to large lateral displacements is still poorly understood. Sand deposits often comprise of many sub-layers as a result of the sedimentation process. A

number of researchers have examined the effect of layering on post-liquefaction sliding including: Scott and Zukerman (1972), Kokusho (1999), Malvick et al. (2002) and Kulasingam (2003). Based on physical model tests and site investigations, Kokusho (1999) and Kokusho and Kojima (2002) demonstrated failure can be caused by the formation of a water film at the base of a sub-layer leading to a zone of essentially zero strength. The water film effect is associated with upward flow of water arising from liquefaction. When such flow is constricted by a lower permeability layer, it results in a void redistribution and an accumulation of pore water that can lead to the formation of a water film. The permeability contrast to cause such an effect can be associated with silt and clay layers or sand and gravel layers, and it is important that these layers be identified in site investigation. Layering and associated void ratio change during and or after an earthquake can explain why the steady-state strength approach can lead to significantly higher values of residual strength than those estimated from back analysis of field case studies (Seed 1987, Byrne and Beaty 1997 and Kokusho 2003).

Our understanding of the behavior of liquefiable soils has increased dramatically in the past 30 years due to:

- Observations from field case histories,
- Extensive laboratory testing of soil elements under monotonic and cyclic loading,
- Model testing of earth structures under simulated earthquake loading, and
- Development of numerical modeling procedures.

Laboratory model testing suggests that slopes comprised of clean loose sands are unlikely to suffer a flow slide, because, although they can be triggered to liquefy, their undrained strengths are generally adequate for stability unless they are very loose. However, if the sands contain low permeability silt layers that impede drainage, a water film and complete loss of strength can occur. Traditionally, drainage conditions in laboratory investigations to characterize liquefiable soils are considered as either undrained or (fully) drained. However, these conditions may not represent the real situation for stratified deposits in the field, because during and after shaking water migrates from zones with higher excess pressure towards zones with lower pressure.

In this paper a dynamic coupled stress-flow analysis procedure is utilized to study the mechanisms involved in large deformations leading to lateral spreads and flow failures in gentle slopes in liquefiable ground. Based on such analyses, implications for design of mitigation methods to resist seismic loading are examined.

2. SAND LIQUEFACTION AND FAILURE

Seismic liquefaction refers to a sudden loss in stiffness and strength of soil due to cyclic loading effects of an earthquake. The loss arises from a tendency for soil to contract under cyclic loading, and if such contraction is prevented or curtailed by the presence of water in the pores that cannot escape, it leads to a rise in pore water pressure and a resulting drop in effective stress. If the effective stress drops to zero (100% pore water pressure rise), the strength and stiffness also drop to zero and the soil behaves as a heavy liquid. However, unless the soil is very loose it will dilate and regain some stiffness and strength, as it strains. If this strength is sufficient, it will prevent a flow slide from occurring, but may still result in excessive displacements commonly referred to as lateral spreading. The potential for lateral spreading and flow slides can greatly increase if low permeability layers e.g. silt layers within a soil deposit impede drainage forming a barrier to flow that can result in an expansion of the sand skeleton and accumulation of pore water at the base of the layers.

The majority of the laboratory element tests conducted to assess liquefaction resistance of sands have been carried out under undrained condition (constant volume). Pore-pressure rise in these elements occur under applied shear stress causing a reduction in effective stresses and strength. Recent experimental studies, Vaid and Eliadorani (1998) and Eliadorani (2000) demonstrate that a small net flow of water into an element causing it to expand results in additional pore pressure generation and further reduction in strength. As a result, soil elements can liquefy due to expansive volumetric strains that cannot be predicted from undrained tests and analyses.

To investigate the effects of low permeability layers on ground deformations due to earthquakes, it is necessary to predict the generation, redistribution, and dissipation of excess pore pressures during and after earthquake shaking. A fundamental approach requires a dynamic coupled stress-flow analysis. In such an analysis, the volumetric strains are controlled by the compressibility of the pore fluid and flow of water through the soil elements. To predict the instability and liquefaction flow, an effective stress approach based on an elastic–plastic constitutive model (UBCSAND model) was used. The model is calibrated against laboratory element data as well as centrifuge data and is described below.

3. STRESS-STRAIN MODEL FOR SAND

The UBCSAND constitutive model is based on the elastic–plastic stress–strain model proposed by Byrne et al. (1995), and has been further developed by Beaty and Byrne (1998) and Puebla (1999). The model has been successfully used in analyzing the CANLEX liquefaction embankments (Puebla et al. 1997) and predicting the failure of Mochikoshi tailings dam (Seid-Karbasi and Byrne 2004). It has also been used to examine dynamic centrifuge test data (e.g. Byrne et al. 2004). It is an incremental elastic–plastic model in which the yield loci are lines of constant stress ratio ($\eta = \tau / \sigma'$). The flow rule relating the plastic strain increment directions is non-associated and leads to a plastic potential defined in terms of dilation angle as shown in Figure 1. The elastic component of response is assumed to be isotropic and

specified by a shear modulus, G^e, and a bulk modulus, B^e, as follows:

$$G^e = K^e_G \, . \, P_a \, (\sigma' / P_a)^{ne} \quad [1]$$

$$B^e = \alpha \, . \, G^e \quad [2]$$

where K^e_G is a shear modulus number, P_a is atmospheric pressure, $\sigma' = (\sigma'_x + \sigma'_y) / 2$, n_e is an elastic exponent approximately 0.5, α depends on Poisson's ratio and ranges from 2/3 to 4/3. The plastic shear strain increment $d\gamma^P$ is related to stress ratio, $d\eta$, where $\eta = \tau / \sigma'$, and can be expressed as:

$$d\gamma^P = (G^P / \sigma')^{-1} \, . \, d\eta \quad [3]$$

Where G^P is the plastic shear modulus and given by a hyperbolic function as:

$$G^P = G^P_i \, . \, (1- (\eta / \eta_f) . R_f)^2 \quad [4]$$

Where G^P_i is the plastic shear modulus at low stress ratio level ($\eta = 0$), η_f is the stress ratio at failure and equals $\sin\varphi_f$, where φ_f is the peak friction angle, and R_f is the failure ratio. The associated increment of plastic volumetric strain, $d\varepsilon_v^P$, is related to the increment of plastic shear strain, $d\gamma^P$, through the flow rule as follows:

$$d\varepsilon_v^P = d\gamma^P \, . \, (\sin\varphi_{cv} - \eta) \quad [5]$$

where φ_{cv} is the friction angle at constant volume or phase transformation. It may be seen that at low stress ratios, significant shear induced plastic compaction is occurring, while no compaction is predicted at stress ratios corresponding to φ_{cv}. For stress ratios greater than φ_{cv}, shear induced plastic expansion or dilation is predicted.

The response of sand is controlled by the skeleton behaviour outlined above. The presence of a fluid (air water mix) in the pores of the sand acts as a volumetric constraint on the skeleton if drainage is fully or partially curtailed. It is this constraint that causes the pore pressure rise that can lead to liquefaction. Provided the skeleton or drained behaviour is appropriately modeled under monotonic and cyclic loading conditions, and the stiffness of the pore fluid and drainage are accounted for, the liquefaction response can be predicted.

This model was incorporated in the commercially available computer code FLAC (Fast Lagrangian Analysis of Continua) Version 4.0 (Itasca 2000). This program models the soil mass as a collection of grid zones or elements and solves the coupled stress flow problem using an explicit time stepping approach.

The key elastic and plastic parameters can be expressed in terms of relative density, Dr, or normalized standard penetration test values, $(N1)_{60}$. Initial estimates of these parameters have been approximated from published data

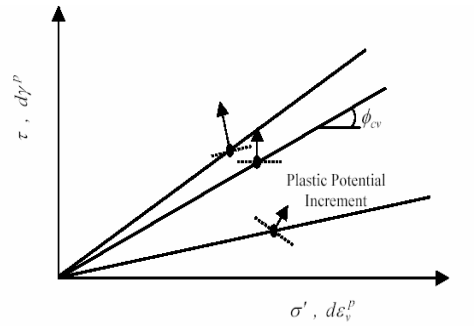

Figure 1: Moving of yield loci with stress ratio.

and model calibrations. The response of sand elements under monotonic and cyclic loading can then be predicted and the results compared with laboratory data. In this way, the model can be made to match the observed response over the range of relative density or $(N1)_{60}$ values.

The model has also been calibrated to reproduce the NCEER 97 triggering chart, which in turn is based on field experience during past earthquakes and is expressed in terms of Standard Penetration Test resistance value, $N1_{(60)}$. The model properties to obtain such agreement are therefore expressed in terms of $N1_{(60)}$.

3.1 Model Simulation of Laboratory Element Tests

The model was applied to simulate cyclic simple shear tests under undrained condition. Figure 2 shows model predictions along with test results on Fraser River sand. The test had an initial vertical consolidation stress σ'_v =100 kPa and Dr=40%. The results in terms of stress-strain, and excess pore pressure ratio, Ru compare reasonably well with the laboratory data. A comparison of model prediction with tests results in terms of required number of cycles to trigger liquefaction for different cyclic stress ratios, CSR is shown in Figure 2c and shows good agreement.

The model was also used to predict the effect of both undrained and partial drainage as observed in triaxial monotonic tests. The partial drainage involved injecting the sample with water to expand its volume as it was sheared. The injection causes a drastic reduction in strength. In the numerical model the same volumetric expansion was applied and the results shown in Figure 3 (model prediction with dotted line) are in remarkably good agreement with the measured data.

The above simulations illustrate that the model can generate the appropriate pore pressures and stress strain response to undrained loading as well as account for the effect of volumetric expansion caused by inflow of water into an element.

4. SOIL PROFILE USED IN THE ANALYSES

The soil profile used in this study is a 24 m thick deposit representing a submarine ground condition. It comprises of

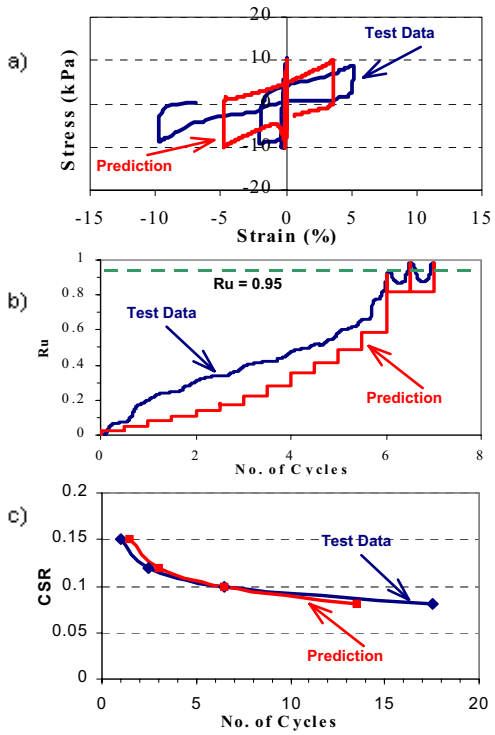

Figure 2. Comparison of predicted and measured response for Fraser River Sand, a) stress-strain, b) & c) Ru & CSR vs. No. of cycles (tests data from Sriskandakumar 2004).

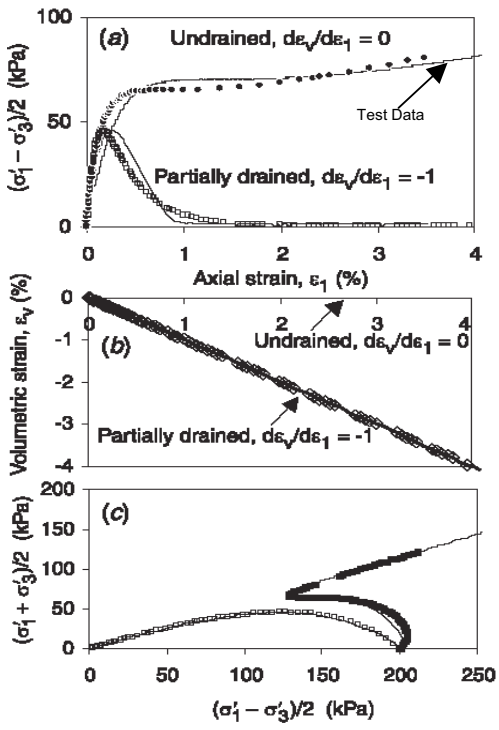

Figure 3. Predictions of element undrained and partially drained triaxial test on Fraser River sand, (a) stress–strain, (b) volumetric strains, and (c) stress paths (from Atigh and Byrne 2004).

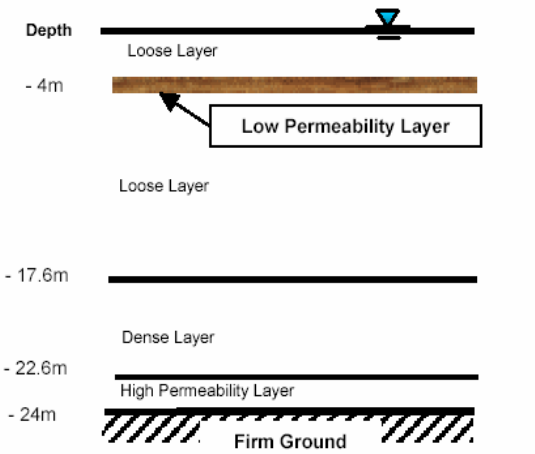

Figure 4: Soil profile used in the analyses

loose sand deposited over a coarse dense sand high permeability layer. The effect of a low permeability layer within the loose sand at a depth of 4 m is examined. The soil profile is illustrated in Figure 4.

Fraser River sand, with relative density Dr= 40 % and 80% are considered to represent the loose and dense layers, respectively. Materials properties are tabulated in Table 1, in which ρ_d, n and k are material dry density, porosity and permeability respectively. UBCSAND model was applied to loose, dense and drain layers with corresponding equivalent UBCSAND $(N1)_{60}$ values. The low permeability silt layer barrier is simulated with a Mohr-Coulomb model with cohesion, C=30 kPa and permeability, k=100 times lower than that of the loose layer.

Input base motion in terms of acceleration time history is shown in Figure 5. It is called A475 event and represents an earthquake event with 10% probability of occurrence in a 50-year return period in the Lower Mainland, BC. Analyses were conducted for two conditions:

1. 1° sloping ground without low permeability layer
2. 1° sloping ground with low permeability layer

5. ANALYSES AND RESULTS

To model the free field condition of the liquefiable ground a mesh with 5 x 25 zones as illustrated in Figure 6 was used. Material types are recognized with different permeability values as shown in the Figure.

5.1 Sloping Ground without Barrier

A sloping ground condition with 1° inclination was analyzed without a low permeability layer. The results in terms of time histories of excess pore pressure ratio, Ru for selected depths are shown in Figures 7 (for position of the points refer to Figure 6). The predicted patterns of excess pore pressure indicate that liquefaction starts from the top and extends to depth. It may be seen that the maximum

Table 1. Materials properties used in the analyses.

Material	ρ_d ($_{1000\ kg/m^3}$)	n	UBCSAND $N_{1(60)}$	k (m/s)
Loose 40%	1.50	0.448	6.2	4.4e-4
Silt barrier	1.50	0.488	----	4.4e-6
Dense 80%	1.60	0.406	21.1	3.2e-4
Drain	1.60	0.406	21.1	3.2e-2

predicted Ru value is approximately 90%. It may also be seen that excess pore pressures dissipate first at depth while remaining high near the surface. A similar trend has been reported from centrifuge tests for level and sloping ground (Taboada and Dobry, 1993a and 1993b).

Figure 8 illustrates the deformation pattern of the soil profile together with displacement vectors. It indicates that most of the lateral displacement occurs in the upper part where Ru is higher, with a maximum value of 1.5 m at top surface. This pattern compares well with centrifuge data (tested at 50g) from Taboada and Dobry (1998) shown in Figure 9. Here profiles of lateral displacement at different time intervals for sloping ground with 5.16° slope are presented (scaling factor, 50). The time history of horizontal displacement of the top surface is shown in Figure 10 It indicates that for the case without the barrier, all displacements occur during shaking and reach their maximum value at the end of excitation.

5.2 Sloping Ground with Barrier

Model including a low permeability layer was next analyzed. This layer was located at a depth of 4m and had a permeability 100 times lower than that of the loose sand. Ground response in terms of excess pore pressure ratio, Ru for different depths are shown in Figure 11. As may be seen, excess pore pressure beneath the barrier layer increases very rapidly and remains high (Ru ≈100%) directly beneath the barrier after the end of shaking, while dissipation occurs at greater depths. It indicates that water flows from the greater depths towards the layer beneath the barrier. This causes higher excess pore pressure that last for a significantly longer time compared to the case without a barrier. The injected flow causes an expansion of the layer beneath the barrier to occur at essentially zero effective stress and leads to large deformation. The deformation pattern after 84 s together with displacement vectors are shown in Figure 12. Comparing the pattern and magnitude of lateral displacements with and without a barrier layer (Figures 12 and 8), it may be seen that the magnitude has increased from 1.5 to 6.4m and the pattern is quite different with a large slippage occurring at the base of the barrier layer. Time histories of horizontal displacement of the top surface are compared with the condition without a barrier layer in Figure 10. It may be seen that the surface displacements are much larger when a barrier layer is present. They are larger during shaking and continue to increase after shaking ceases.

Table 2 summarizes the effects of the low permeability layer on lateral displacements. It shows that a large portion of the surface displacements occurs after

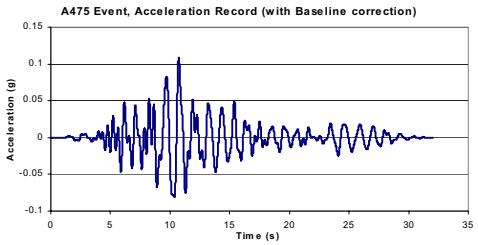

Figure 5. Acceleration time history for A475 event

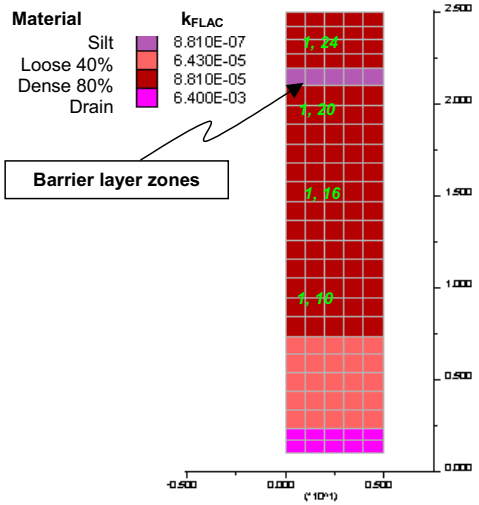

Figure 6. Different materials within the mesh

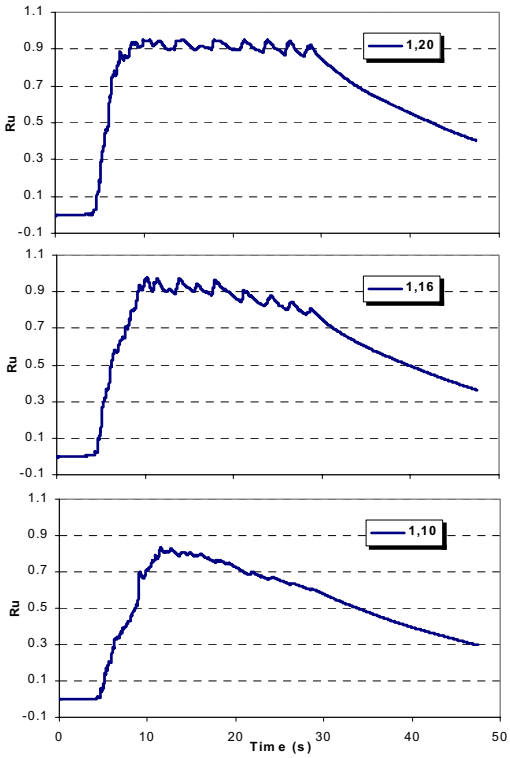

Figure 7. Excess pore pressure ratio Ru vs. time at selected points with increasing depth.

Table 2. Barrier effects on lateral displacements.

x-displacement	No barrier	With barrier
Top surface max. x-disp. (m)	1.6	6.4
Max. x-disp. below barrier (m)	1.2	0.8
Top surface x-disp. at 30s (m)	1.6	3.5
x-disp. below barrier at 30s (m)	1.6	0.8
Ratio of x-disp. over and below barrier	50%	12.5%
Ratio of post earthquake x-disp. to total	0.0%	45%

earthquake shaking due to the time required for water to flow into to the layer beneath the barrier. Lateral displacements beneath the barrier are less than that of the case without the barrier. Similar analyses were also carried out for the same soil profile including barrier layer with zero slope (level ground). For the case of the level ground, negligible lateral displacements are predicted.

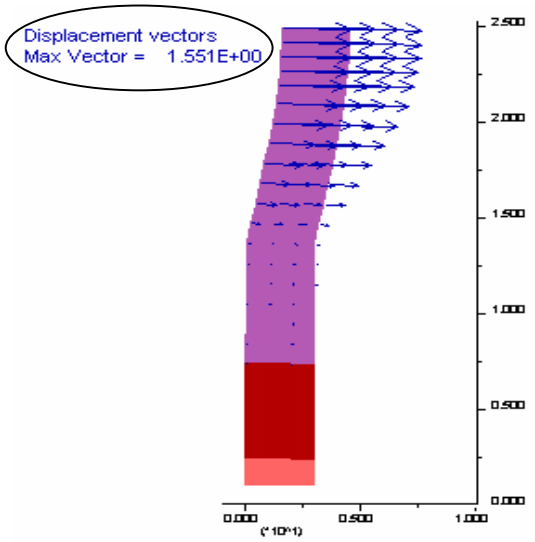

Figure 8. Deformation pattern of the soil profile (with maximum lateral displacement of 1.5 m).

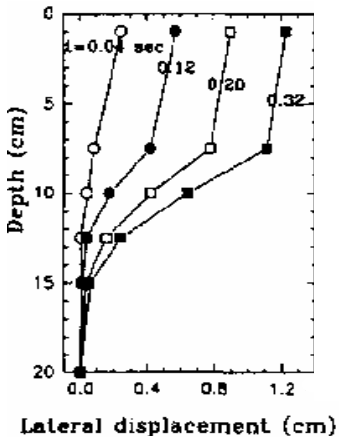

Figure 9. Lateral displacement pattern measured in centrifuge test for a 10m thick sloping ground (model scale).

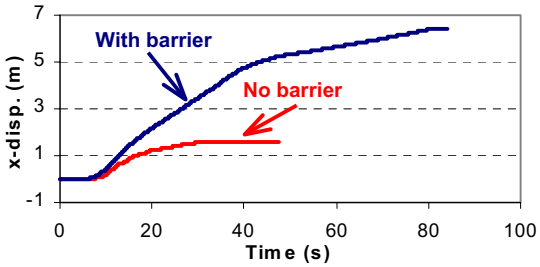

Figure 10. Surface lateral displacement vs. time.

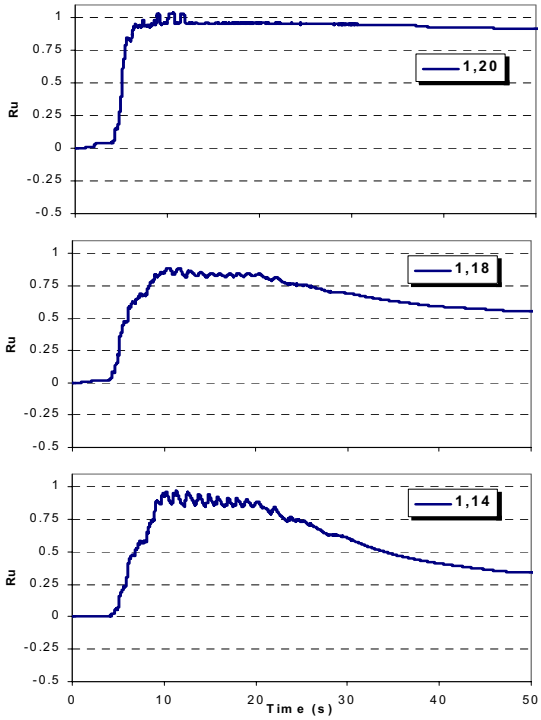

Figure 11. Excess pore pressure ratio Ru vs. time at selected points with increasing depth.

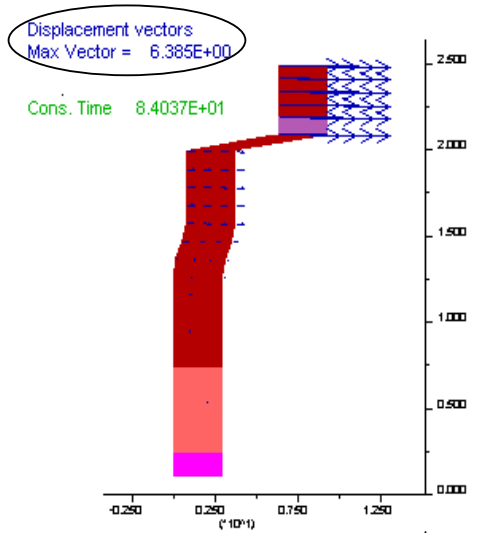

Figure 12. Deformation pattern of the soil profile (with maximum lateral displacement of 6.4 m).

6. COUNTER MEASURES FOR FLOW FAILURE

Drains have the potential to nullify the barrier effect and curtail or prevent the occurrence of lateral spread or flow slides in the event of an earthquake. They can facilitate dissipation of excess pore pressure and mitigate the impedance effects of low permeability layers. This is examined for the same profile with 1.0° inclination. Figure 13a shows the model with a drain column 100 times more permeable than the loose sand. Figure 13b shows distributions of excess pore pressure ratio, Ru within the model along with flow vectors after 12 seconds of shaking. It is seen that Ru increases with distance from the drain column. The column drain has some excess pore pressure during shaking. The maximum predicted lateral displacement in this case was negligible (0.06m) even compared with that of the model without low permeability layer. A similar effect for drains is reported by Rathje et al. (2004) based on physical model tests.

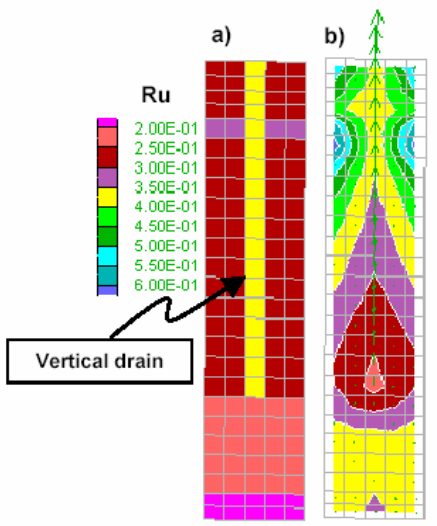

Figure 13. Treated model a) central vertical drain b) Ru and flow vectors at 12 s.

7. CONCLUSIONS

Submarine slides have been reported during past earthquake worldwide. A number of civil structures and soil deposits in coastal or river areas have suffered large deformations during past earthquakes as a result of soil liquefaction. The deformations may exceed several meters even in gentle slopes of less than a few percent. Lateral spreads or flow slides occur not only during but also after earthquake shaking. Clean loose sands are unlikely to suffer a flow slide, although they can be triggered to liquefy, their undrained strengths are generally adequate for stability unless they are very loose. However, if the sands contain low permeability layers that impede drainage, a water film and or void redistribution may cause complete loss of strength of the soil directly beneath that layer.

In the paper a numerical approach that captures element sand behavior in monotonic and cyclic loading under different drainage conditions; undrained and partially drained was utilized to study the effects of low permeability layers on sloping ground response during earthquake loading. The following conclusions are based on the analyses:

- Presence of a low permeability layer in a gentle slope comprising liquefiable soils can result in a large lateral spread or flow slide. Such layers may have caused the delayed failures observed during past earthquakes.
- Most of the relative movements occur at the base of the low permeability sub-layer. Maximum displacements occur near the surface above the barrier layer.
- A large part of the deformations occur some time after shaking has ceased, depending on the time needed for migration of water from zones with higher excess pore pressures.
- Installation of vertical drains can mitigate the destructive effects of low permeability layers. This has been demonstrated in these analyses and has been observed from model tests.
- The design of these drains can be assessed from dynamic coupled flow effective stress analyses using appropriate modeling parameters and design input motions. The dimensions and location of remediation measures can be optimized from dynamic analyses.
- Appropriate site investigation methods should be used to detect possible thin layers of low permeability within sand deposits.

8. ACKNOWLEDGEMENTS

The authors acknowledge the financial support from BC Hydro through the Professional Partnership program and the support of the National Scientific and Engineering Research Council through Strategic Liquefaction Grant No. NSERC 246394, and NSERC COSTA No. 03608-CG068625. The authors also acknowledge the contribution of Mr. Ernest Naesgaard in demonstrating that the UBCSAND model could simulate the water film effect.

9. REFERENCES

Atigh, E. and Byrne, P. M. 2004. Liquefaction flow of submarine slopes under partially undrained conditions: an effective stress approach. Can. Geotechnical J., V. 41, pp. 154-165.

Berrill, S. A,, Christensen, S. A., Keenan R. J., Okada, W. and Pettinga, J. R., 1997. Lateral-spreading loads on a piled bridge foundation. Proc., Discussion Session, Seismic Behavior of Ground and Geotechnical Structures, ICSMGE, Humburg, pp. 173–83.

Beaty, M. H. and Byrne, P. M. 1998. An Effective stress model for predicting liquefaction behavior of sand. Proc., Specialty Conf., Geotechnical Earthquake

Engineering and Soil Dynamics III, Seatle, ASCE G.S.P No. 75, V. 1, pp. 766-777.

Byrne, P. M., and Beaty, M. H. 1997. Post-liquefaction shear strength of granular soils: theoritical/conceptual issues. Proc., Workshop on Post-Liquefaction Shear Strength of Granular Soils, Urbana-Champion, Illinois, pp. 16-45.

Byrne, P.M., Roy, D., Campanella, R.G., and Hughes, J. 1995. Predicting liquefaction response of granular soils from pressuremeter tests. ASCE National Convention, ASCE, GSP 56, pp. 122-135.

Byrne, P.M., Park, S., Beaty, M., Sharp, M., Gonzalez, L. and Abdoun, T., 2004. Numerical modeling of liquefaction and comparison with centrifuge tests. Can Geotechnical J., V. 41, pp. 193-211.

Coulter H. W, and Migliaccio R. R., 1966. Effects of the Earthquake of March 27, 1964 at Valdez, Alaska, Geological Survey Professional Paper 542-C, US Department of the Interior, p. 36.

Eliadorani, A. A. 2000. The response of sands under partially drained states with emphasis on liquefaction. PhD. thesis, Civil Engg. Dept., The University of British Columbia, Vancouver, B.C.

Field M. E., Gardner J. V., Jennings A. E., and Edwards B. D. 1982. Earthquake induced sediment failures on a 0.258 slope, Klamath River Delta. J. California. Geology, V.10, pp. 542–546.

Hamada, M. 1992. Large ground deformations and their effects on lifelines: 1964 Niigata Earthquake. Proc., Lifeline Performance During Past Earthquakes, V. 1: Japanese Case Studies Tech. Rep. NCEER-92-0001, National Center for Earthquake Engineering Research, Buffalo, N.Y., 3/1–3/123.

Hampton, M. A. and Lee H. J., 1996. Submarine and landslides. J., Review of Geophysics, V. 34, pp.33-39.

Ishihara, K. 1984. Post-earthquake failure of a tailings dam due to liquefaction of the pond deposit. Proc., Inter. Conf., Case Histories in Geotechnical Engineering, Rolla, Missouri, V. 3, pp. 1129-1143.

ITASCA, 2000. Fast lagrangian analysis of continua (FLAC), Version 4, User's Guide. Itasca Consulting Group, Inc., Thrasher Square East, 708 South Third Street, Suite 310, Minneapolis, Minnesota.

Kawakami, F. and Asada, A., 1966. Damage to the ground and earth-structures by the Niigata earthquake of June 16, 1964. J., Soils & Foundations, V. 1(1), pp.14–30.

Kokusho, T., 1999. Water film in liquefied sand and its effect on lateral spread. J. Geotechnical and Geo-environmental Engineering, ASCE, V. 125(10), pp. 817–826.

Kokusho, T. and Kojima T., 2002. Mechanism for post-liquefaction water film generation in layered sand. J. Geotechnical and Geo-environmental Engineering, ASCE, V. 128(2), pp. 129–37.

Kokusho, T., 2003. Current state of research on flow failure considering void redistribution in liquefied deposits. J., Soil Dynamic and Earthquake Engineering, V. 23, pp. 585–603.

Kulasingam, R., 2003. Effects of void redistribution on liquefaction-induced deformations. PhD thesis, Civil & Environmental Engg. Dept, U.C., Davis. Cal.

Lemke, R. W., 1967. Effects of the earthquake of March 27, 1964 at Seward, Alaska. Geological Survey Professional Paper 542-E, US Department of Interior.

Malvick, E. J., Kulasingam, R., Kutter, B. L., and Boulanger, R. W., 2002. Void redistribution and localized shear strains in slopes during liquefaction. Proc. Int. Conf., Physical Modeling in Geotechnics, ICPMG '02, St. John's, NF, Canada, pp. 495-500.

Puebla, H., 1999. A constitutive model for sand analysis of the CANLEX embankment. PhD. Thesis, Civil Engg. Dept., University of British Columbia, Vancouver, B.C.

Puebla, H., Byrne, P. M., and Phillips, R., 1997. Analysis of CANLEX liquefaction embankment: prototype and centrifuge models. Canadian Geotechnical J., 34, pp. 641-654.

Rathje, E. M., Chang, W. J., Cox, B. R., and Stokoe II, K. H., 2004. Effect of prefabricated vertical drains on pore pressure generation in liquefiable sand. Proc., 11th Int. Conf., Soil Dynamics & Earthquake Engineering, UC, Berkeley, V. 2, pp. 529-536.

Scott, R. F., and Zuckerman K. A., 1972. Sand blows and liquefaction in the Great Alaskan Earthquake of 1964. Engineering Publication 1606; National Academy of Sciences, Washington, D.C., pp 170-189.

Seed, H. B., 1987. Design problems in soil liquefaction. J., Geotechnical Engineering, ASCE, V.113 (8), pp. 827-845.

Seid-Karbasi, M. and Byrne, P. M., 2004. Embankment dams and earthquakes. Hydropower and Dams J., V.11(2), pp. 96-102.

Sriskandakumar, S., 2004. Cyclic loading response of Fraser River Sand for numerical models simulating centrifuge tests. M.A.Sc. thesis, Civil Engg. Dept., the University of British Columbia, Vancouver, B.C.

Taboada, V. and Dobry, R., 1993a. Experimental Results of Model No.1 at RPI. Proc., Int. Conf., Verification of Numerical Procedures for the Analysis of Soil Liquefaction Problems (VELACS), U.C, Davis 1993, V. 1, pp. 3-17.

Taboada, V. and Dobry, R., 1993b. Experimental Results of Model No. 2 at RPI. Proc., Int. Conf., Verification of Numerical Procedures for the Analysis of Soil Liquefaction Problems (VELACS), U.C, Davis 1993, V. 1, pp. 277-294.

Taboada, V. and Dobry, R., 1998. Centrifuge modeling of earthquake-induced lateral spreading in sand. J., Geotechnical Engineering, ASCE, 124(12), pp. 1195–206.

Vaid, Y. P., and Eliadorani, A., 1998. Instability and liquefaction of granular soils under undrained and partially drained states. Canadian Geotechnical J., V. 35, pp. 1053–1062.